

Introduction to SAR Interferometry

Erika Podest

30 November 2017

Learning Objectives

By the end of this presentation, you will be able to:

- Understand the basic physics of SAR interferometry
- Describe what SAR interferometric phase tells about the land surface
- Describe the necessary data preprocessing
- Understand the information content in SAR interferometric images

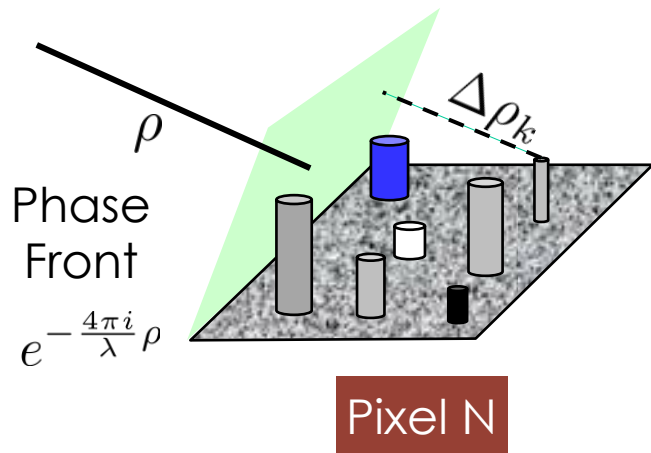




SAR Interferometry Theory

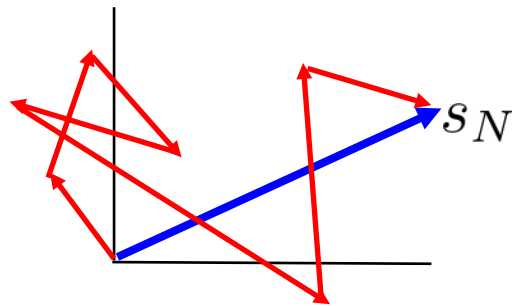
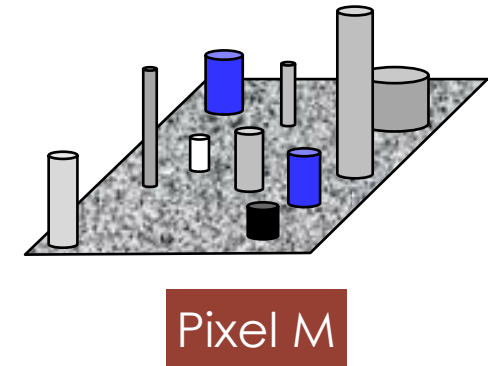
SAR Imagery and Speckle

- Full resolution SAR imagery has a grainy appearance called **speckle**, which is a phenomena due to the coherent nature of SAR imaging

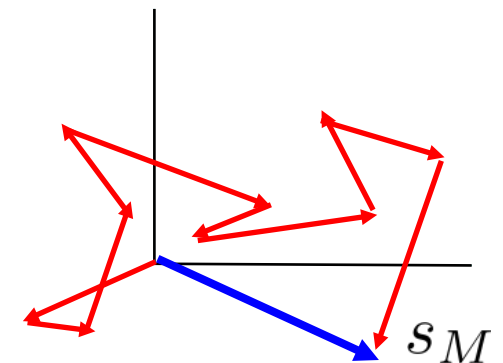


Number and arrangement of scattering elements within resolution cell varies from pixel to pixel

Returned signal is a coherent combination of the returns from the scattering elements.



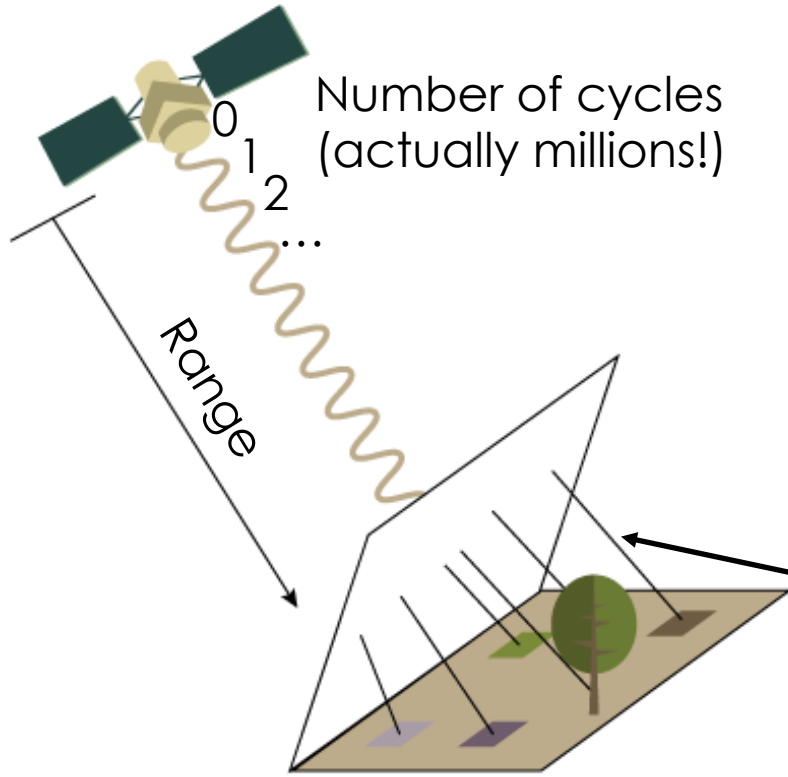
$$s = A \underbrace{e^{-\frac{4\pi i}{\lambda} \rho}}_{\text{Range Phase}} \underbrace{\sum_{k=1}^N a_k e^{-\frac{4\pi i}{\lambda} \Delta \rho_k}}_{\text{Scatterer Contribution}}$$



Slide courtesy of Paul Rosen (JPL)



SAR Phase: A Measure of the Range and Surface Complexity



- The phase of the radar signal is the number of *cycles of oscillation* that the wave executes between the radar and the surface and back again
- The total phase is two-way range measured in wave cycles + random component from the surface
- Collection of random path lengths jumbles the phase of the echo
- Only interferometry can sort it out!

Slide courtesy of Paul Rosen (JPL)



Simplistic View of SAR Phase

Phase of Image 1 $\phi_1 = \frac{4\pi}{\lambda} \cdot \rho_1 + \text{other constants} + n_1$

Phase of Image 2 $\phi_2 = \frac{4\pi}{\lambda} \cdot \rho_2 + \text{other constants} + n_2$

1. The “other constants” cannot be directly determined
2. “Other constants” depend on scatterer distribution in the resolution cell, which is unknown and varies from cell to cell
3. Only way of observing the range change is through interferometry (cancellation of “other constants”)

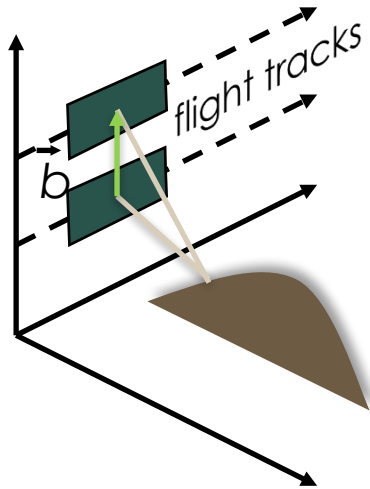
Slide modified from Paul Rosen (JPL)

Types of Radar Interferometry

- Two main classes of interferometric radars are separated based on the geometric configuration of the baseline vector:
 - Interferometers are used for topographic measurements when the antennas are separated in the cross-track direction
 - Interferometers are used to measure line-of-sight motion when the antennas are separated in the along-track direction
 - A single antenna repeating its path can form an interferometer to measure long-term deformation

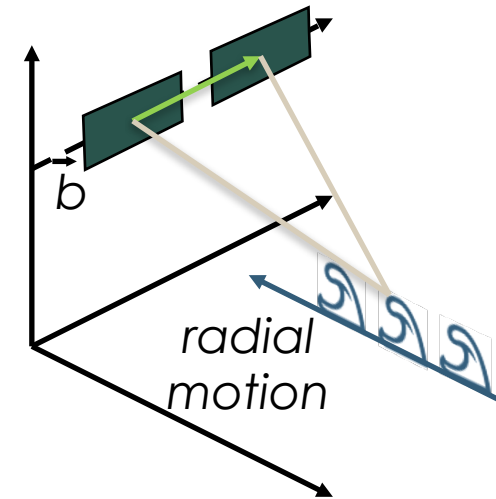
Types of Radar Interferometry

Cross-Track Interferometer



- Dual antenna single pass interferometers
- Single antenna repeat pass interferometers
 - **Topography and Deformation**

Along-Track Interferometer



- Dual antenna single pass interferometers
- Along-track separation
 - **Radial velocity**

Slide modified from Paul Rosen (JPL)



SAR Interferometry Applications: Mapping & Cartography

- Radar Interferometry from airborne platforms is routinely used to produce topographic maps as digital elevation models (DEMs)
 - 2 – 5 meter circular position accuracy
 - 5 – 10 m post spacing and resolution
 - 10 km by 80 km DEMs produced in 1 hr on mini-supercomputer
- Radar imagery is automatically geocoded, becoming easily combined with other (multispectral) datasets
- Applications of topography enabled by interferometric rapid mapping
 - Land use management, classification, hazard assessment, intelligence, urban planning, short and long time scale geology, hydrology

Slide modified from Paul Rosen (JPL)



SAR Interferometry Applications: Deformation Mapping & Change Detection

- Repeat Pass Radar Interferometry from spaceborne platforms is routinely used to produce topographic change maps as digital displacement models (DDMs)
 - 0.3 – 1 cm relative displacement accuracy
 - 10 – 100 m post spacing and resolution
 - 100 km by 100 km DDMs produced rapidly once data is available
- Applications include
 - Earthquake and volcano monitoring and modeling, landslides and subsidence
 - Glacier and ice sheet dynamics
 - Deforestation, change detection, disaster monitoring

Slide modified from Paul Rosen (JPL)



Interferometry for Topography

Measured phase difference:

$$\Delta\phi = -\frac{2\pi}{\lambda}\delta\rho$$

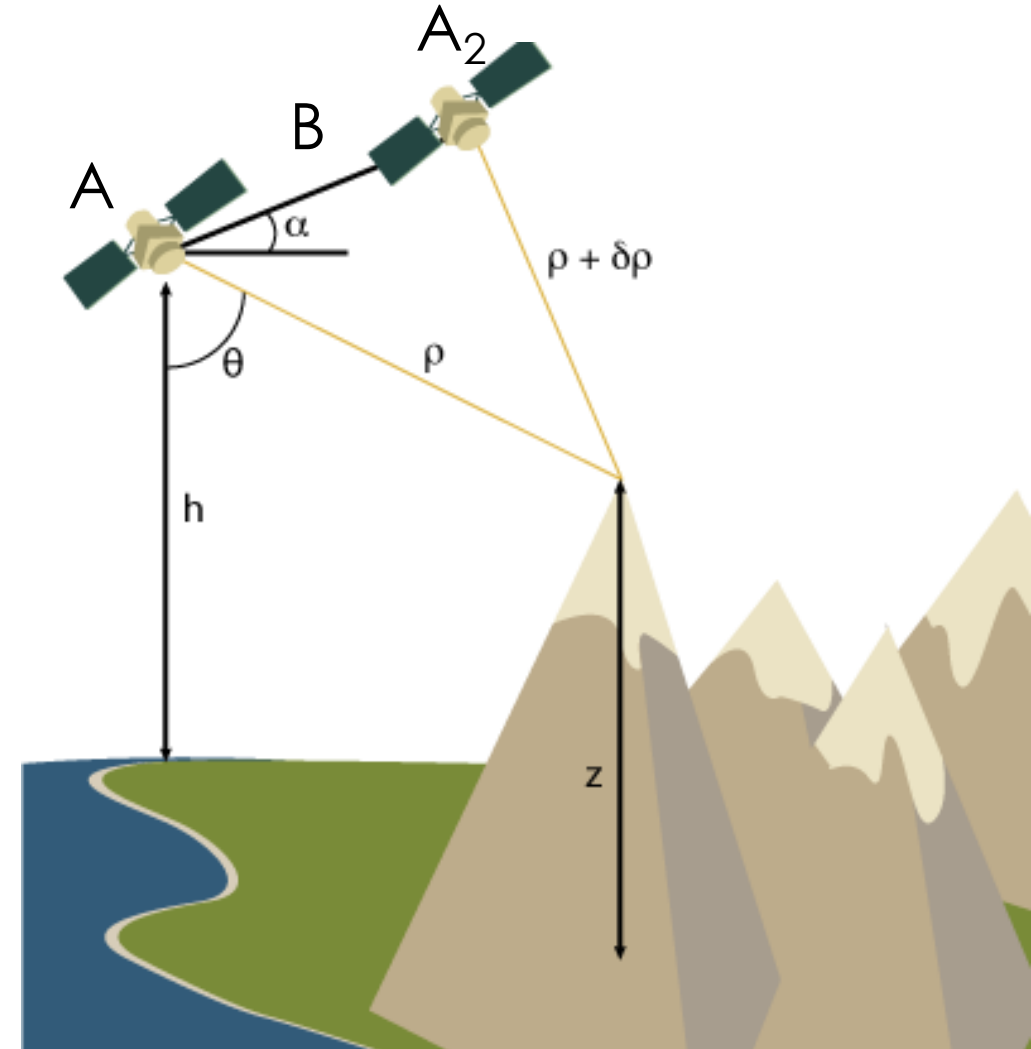
Triangulation

$$\sin(\theta - \alpha) = \frac{(\rho + \delta\rho)^2 - \rho^2 - B^2}{2\rho B}$$

$$z = h - \rho\cos\theta$$

Critical interferometer knowledge:

- baseline ($B\alpha$) to mm's
- System phase differences, to degrees



Slide modified from Paul Rosen (JPL)

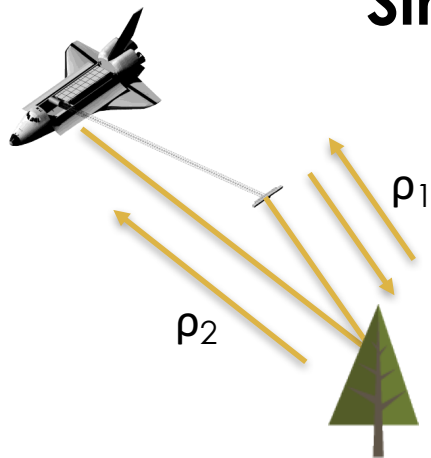


Data Collection Options

For single pass interferometry (SPI) both antennas are located on the same platform, which is ideal for measuring topography. Two modes of data collection are common:

- single-antenna-transmit mode: one antenna transmits and both receive
- ping-pong mode: each antenna transmits and receives its own echoes, effectively doubling the physical baseline

Single-Antenna



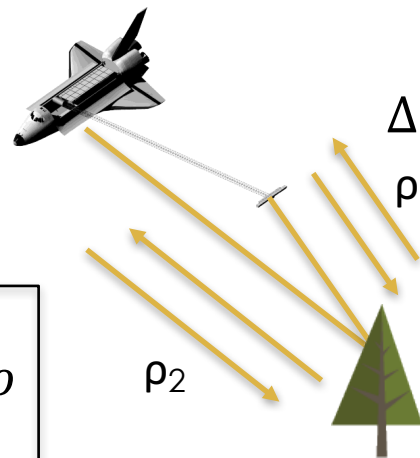
$$\Delta\phi = \frac{2\pi}{\lambda}(\rho_2 + \rho_1) - \frac{2\pi}{\lambda}(\rho_1 + \rho_1)$$

$$= \frac{2\pi}{\lambda}(\rho_2 - \rho_1)$$

$$\Delta\phi = \frac{2\pi\rho}{\lambda} \delta\rho$$

$\rho=1$

Ping-Pong



$$\Delta\phi = \frac{2\pi}{\lambda}(\rho_2 + \rho_1) - \frac{2\pi}{\lambda}(\rho_1 + \rho_1)$$

$$= \frac{4\pi}{\lambda}(\rho_2 - \rho_1)$$

$$\Delta\phi = \frac{2\pi\rho}{\lambda} \delta\rho$$

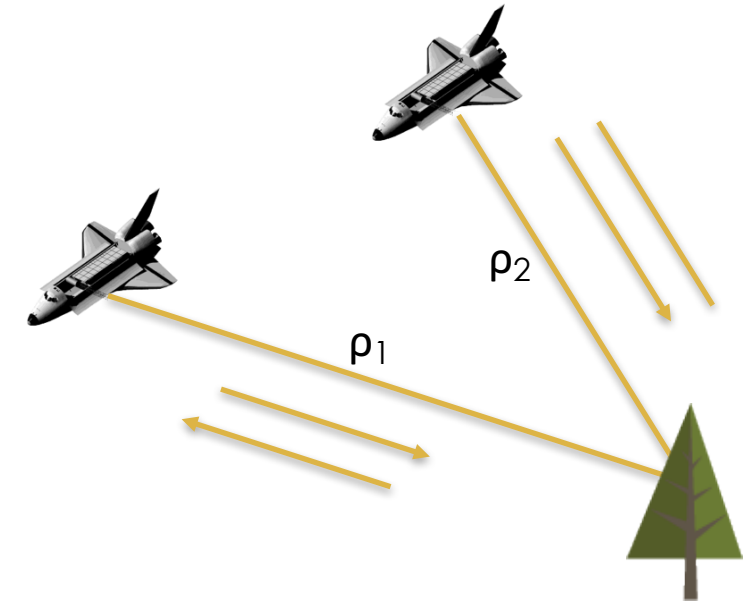
$\rho=2$

Slide modified from Paul Rosen (JPL)



Data Collections Options II

- Interferometric data can also be collected in the repeat pass mode (RPI)
- Two spatially close radar observations of the same scene are made at different times
 - The time interval may range from seconds to years
 - may be made with different sensors provided they have nearly identical radar system parameters
- This kind of data can be used for topography or surface deformation measurements



$$\begin{aligned}\Delta\phi &= \frac{2\pi}{\lambda}(\rho_2 + \rho_1) - \frac{2\pi}{\lambda}(\rho_1 + \rho_1) \\ &= \frac{4\pi}{\lambda}(\rho_2 - \rho_1)\end{aligned}$$

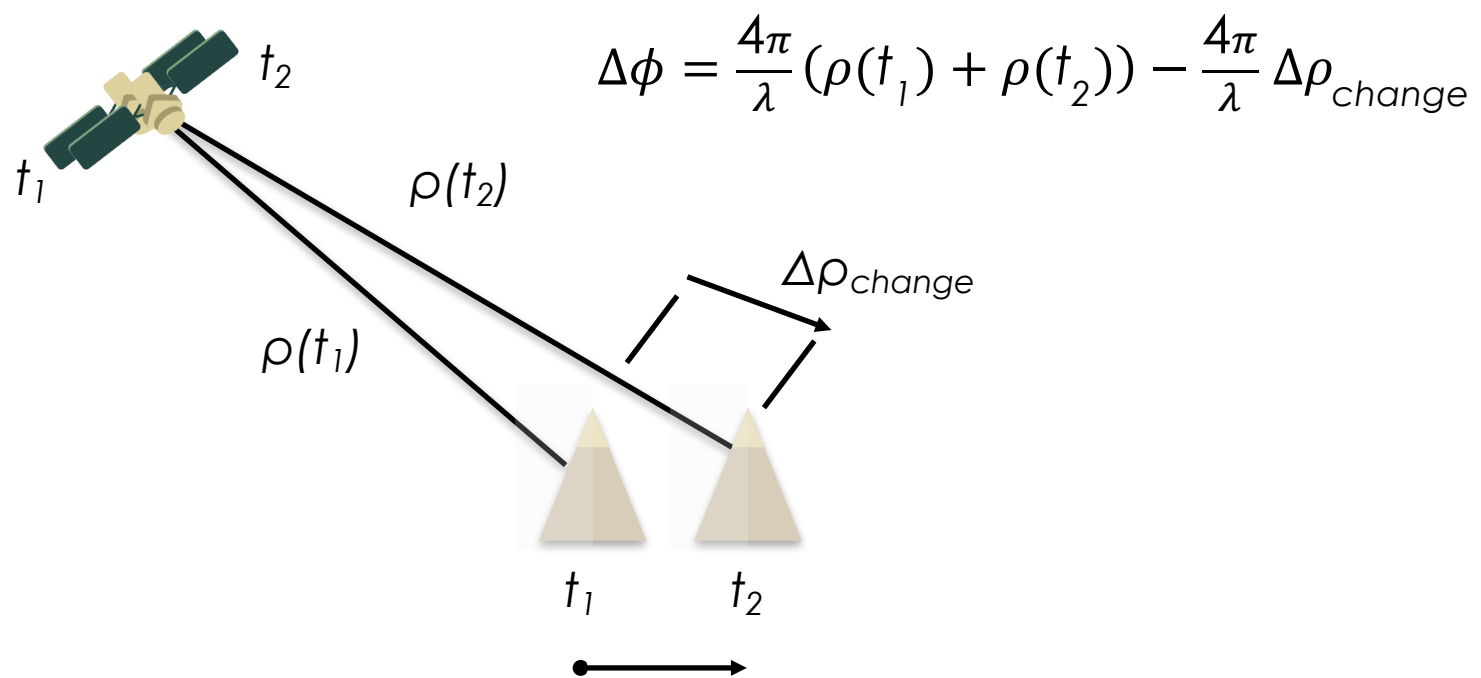
$$\begin{aligned}\Delta\phi &= \frac{2\pi\rho}{\lambda}\delta\rho \\ \rho &= 2\end{aligned}$$

Slide modified from Paul Rosen (JPL)

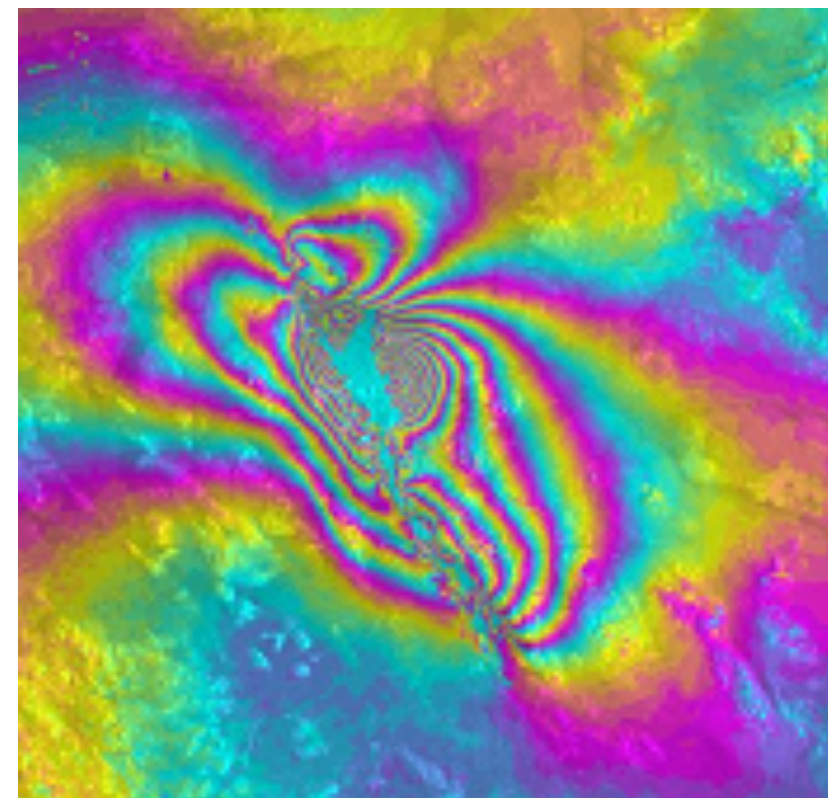


Differential Interferometry

- When two observations are made from the same location in space but at different times, the interferometric phase is directly proportional to any change in the range of a surface feature



Hector Mine Earthquake

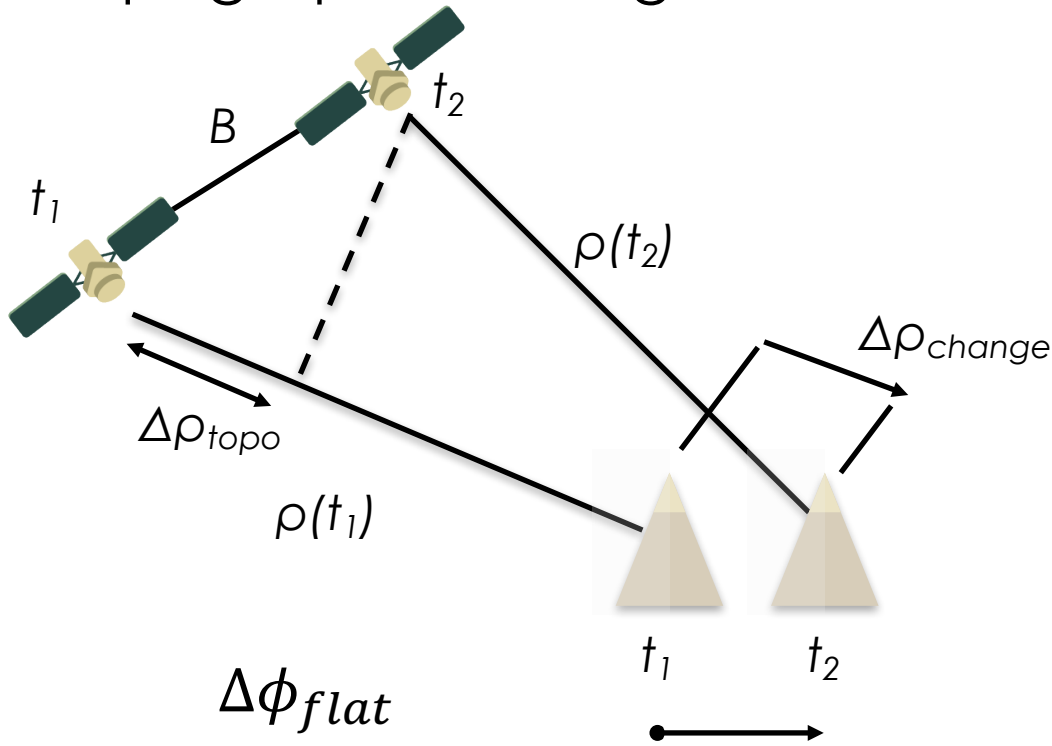


Slide modified from Paul Rosen (JPL)



Differential Interferometry & Topography

- Generally two observations are made from different locations in space and at different times, so the interferometric phase is proportional to topography and topographic change



$$\Delta\phi = \frac{4\pi}{\lambda} \left(-\langle \hat{l}, \vec{b} \rangle + \langle \hat{l}, \vec{D} \rangle \right)$$

↑ topography term ↑ change term

$$\Delta\phi = \frac{4\pi}{\lambda} (\Delta\rho_{change} - \Delta\rho_{topo})$$

$$\Delta\phi = \frac{4\pi}{\lambda} (\Delta\rho_{change} - B \sin(\theta - \alpha))$$

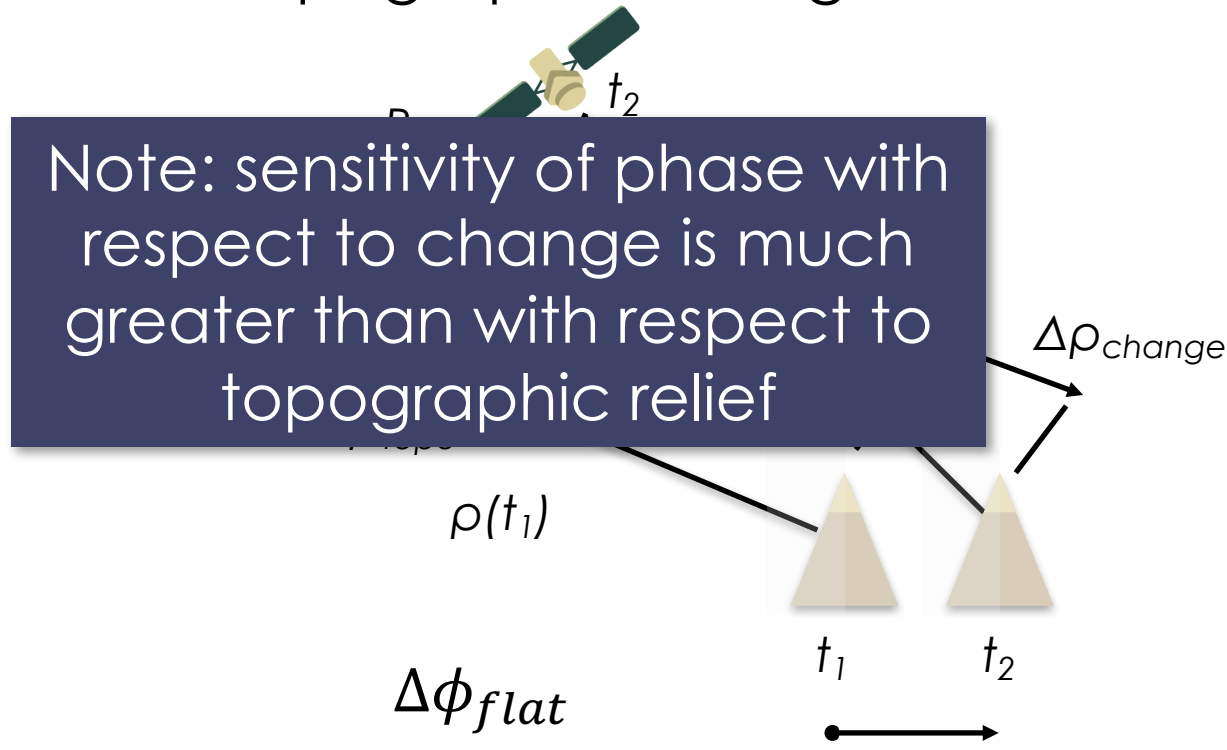
$$\Delta\phi_{flat} = \frac{4\pi}{\lambda} \left(\Delta\rho_{change} - \frac{B_{\perp} h_T}{\rho \sin \theta} \right)$$

Slide modified from Paul Rosen (JPL)



Differential Interferometry & Topography

- Generally two observations are made from different locations in space and at different times, so the interferometric phase is proportional to topography and topographic change



$$\Delta \phi = \frac{4\pi}{\lambda} \left(-\langle \hat{l}, \vec{b} \rangle + \langle \hat{l}, \vec{D} \rangle \right)$$

topography term change term

if topography is known, the second term can be eliminated to reveal surface change

$$\Delta \phi = \frac{4\pi}{\lambda} (\Delta \rho_{change} - B \sin(\theta - \alpha))$$

$$\Delta \phi_{flat} = \frac{4\pi}{\lambda} \left(\Delta \rho_{change} - \frac{B_{\perp} h_T}{\rho \sin \theta} \right)$$

Slide modified from Paul Rosen (JPL)



Differential Interferometry Sensitivities

The reason differential interferometry can detect millimeter level surface deformation is that the **differential phase is much more sensitive to displacements than to topography**

$$(\phi \Leftrightarrow \Delta\phi)$$

$$\frac{\partial\phi}{\partial h} = \frac{2\pi B \cos(\theta - \alpha)}{\lambda \rho \sin \theta} = \frac{2\pi b_{\perp}}{\lambda \rho \sin \theta}$$

Topographic Sensitivity

$$\frac{\partial\phi}{\partial\Delta\rho} = \frac{4\pi}{\lambda}$$

Displacement Sensitivity

$$\sigma_{\phi_{topo}} = \frac{\partial\phi}{\partial h} \sigma_h = \frac{4\pi}{\lambda} \frac{b_{\perp}}{\rho \sin \theta} \sigma_h$$

Topographic Sensitivity Term

$$\sigma_{\phi_{disp}} = \frac{\partial\phi}{\partial\Delta\rho} \sigma_{\Delta\rho} = \frac{4\pi}{\lambda} \sigma_{\Delta\rho}$$

Displacement Sensitivity Term

Slide modified from Paul Rosen (JPL)



Differential Interferometry Sensitivities

The reason differential interferometry can detect millimeter level surface deformation is that the **differential phase is much more sensitive to displacements than to topography**

$$(\phi \Leftrightarrow \Delta\phi)$$

$$\frac{\partial\phi}{\partial h} = \frac{2\pi B \cos(\theta - \alpha)}{\lambda\rho \sin\theta} = \frac{2\pi b_{\perp}}{\lambda\rho \sin\theta}$$

$$\frac{\partial\phi}{\partial\Delta\rho} = \frac{4\pi}{\lambda}$$

$$\sigma_{\phi_{topo}} = \frac{\partial\phi}{\partial h} \sigma_h = \frac{4\pi}{\lambda} \frac{b_{\perp}}{\rho \sin\theta} \sigma_h$$

$$\sigma_{\phi_{disp}} = \frac{\partial\phi}{\partial\Delta\rho} \sigma_{\Delta\rho} = \frac{4\pi}{\lambda} \sigma_{\Delta\rho}$$

$$\text{Since } \frac{b}{\rho} \ll 1 \rightarrow \frac{\sigma_{\phi_{disp}}}{\sigma_{\Delta\rho}} \gg \frac{\sigma_{\phi_{topo}}}{\sigma_h}$$

Meter scale topography measurement –
millimeter scale topographic change

Slide modified from Paul Rosen (JPL)



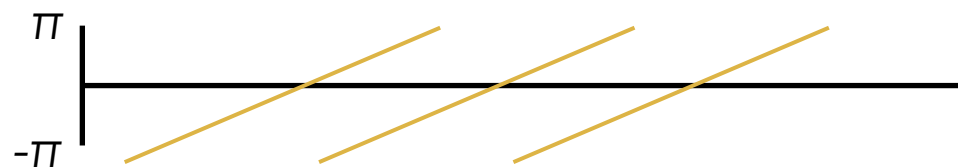
Phase Unwrapping

From the measured, wrapped phase, unwrap the phase from some arbitrary starting location, then determine the proper 2π phase “ambiguity”

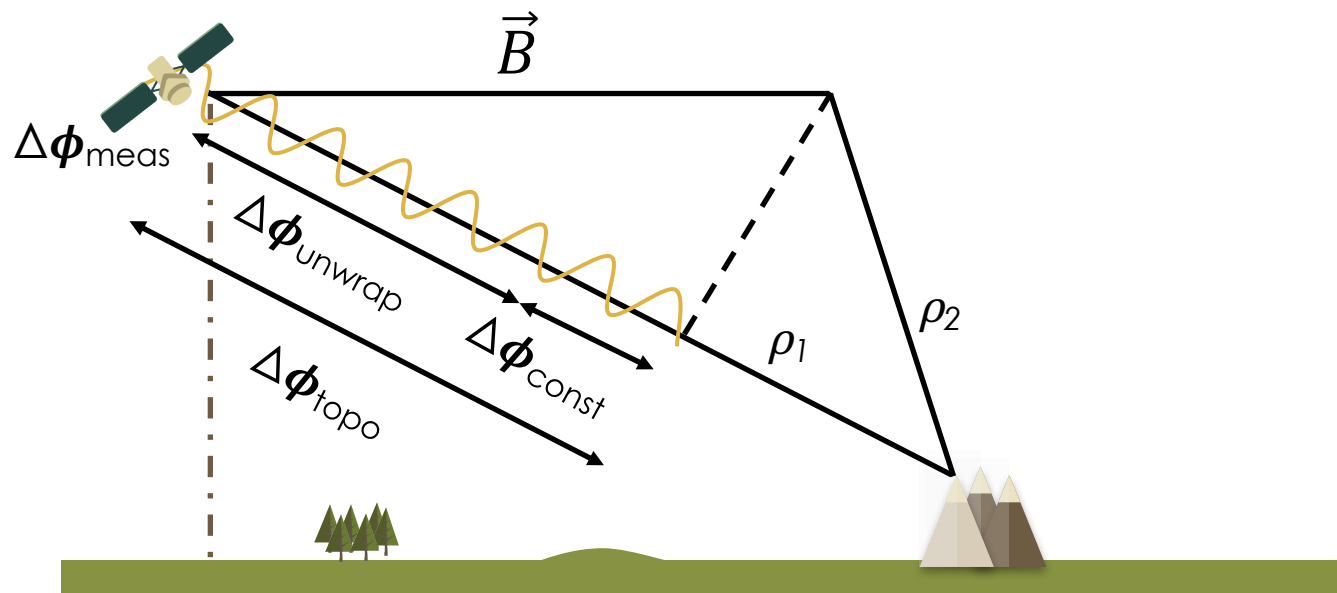
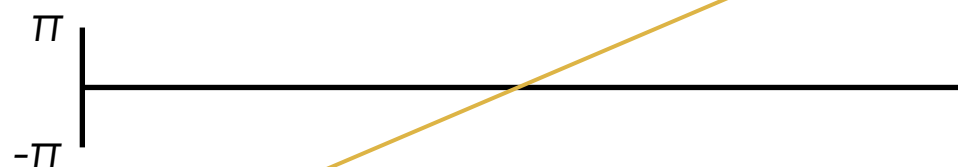
Actual phase



Wrapped (measured) phase



Typical unwrapped phase



$$\Delta\phi_{topo} = \frac{2\pi\rho}{\lambda} (\rho_1 - \rho_2) = \frac{2\pi\rho}{\lambda} \vec{B} \cdot \vec{l}$$

$$\Delta\phi_{meas} = \text{mod}(\Delta\phi_{topo}, 2\pi)$$

$$\Delta\phi_{unwrap}(s, \rho) = \Delta\phi_{topo}(s, \rho) + \Delta\phi_{const}$$



Correlation* Theory

- InSAR signals decorrelate (become incoherent) due to:
 - thermal and processor noise
 - differential geometric and volumetric scattering
 - rotation of viewing geometry
 - random motions over time
- Decorrelation relates to the local phase standard deviation of the interferogram phase
 - affects height and displacement accuracy
 - affects ability to unwrap phase

**correlation and coherence are often used synonymously*

Slide modified from Paul Rosen (JPL)



InSAR Correlation Components

- Correlation effects multiply, unlike phase effects that add
- Low coherence or decorrelation for any reason causes a loss of information in that area

$$\gamma = \gamma_v \gamma_g \gamma_t \gamma_c$$

where

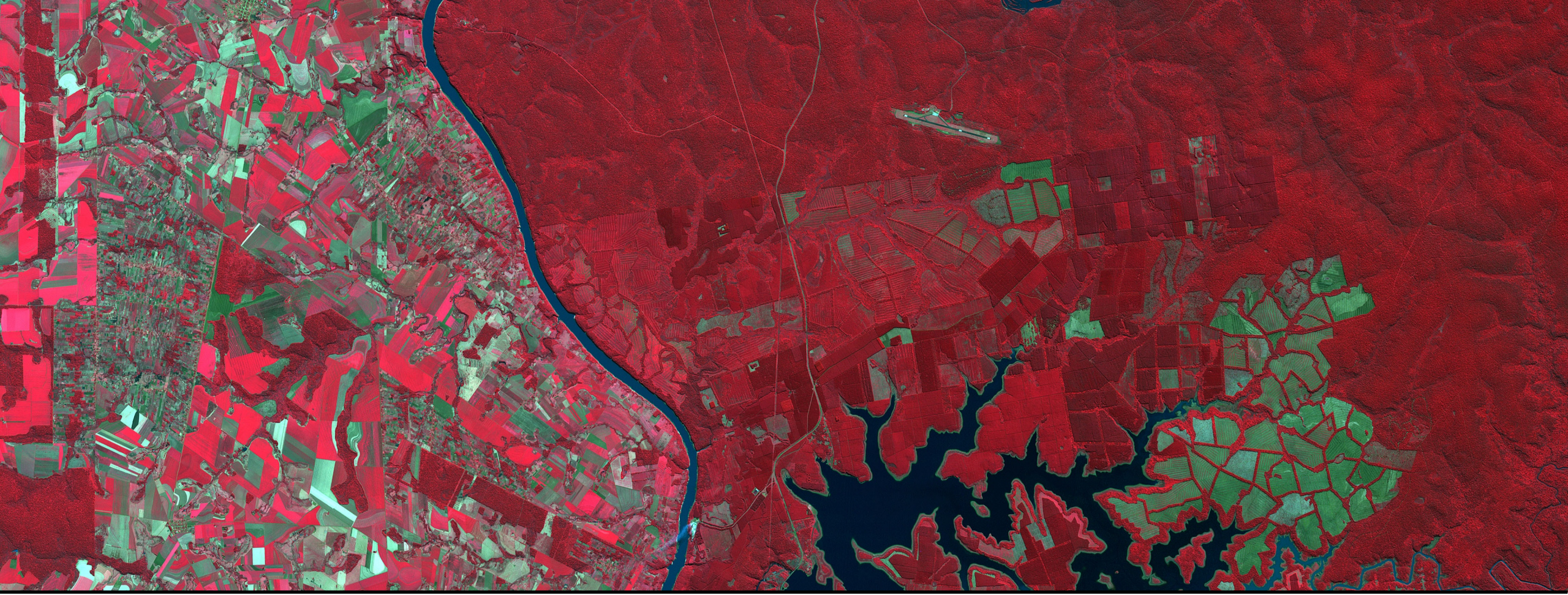
γ_v is volumetric (trees)

γ_g is geometric (steep slopes)

γ_t is temporal (gradual changes)

γ_c is sudden changes

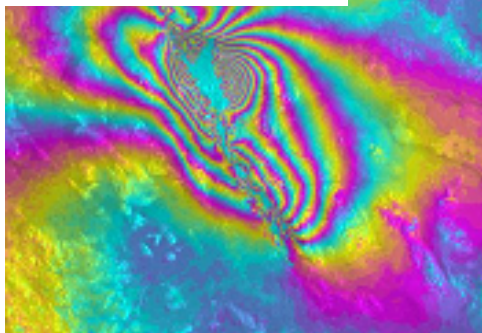




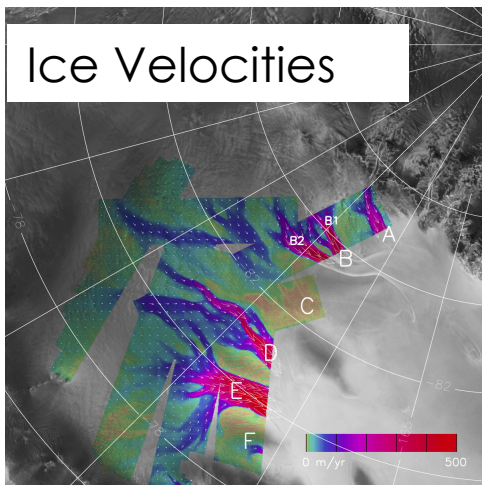
InSAR Applications

Examples of Deformation

Hector Mine Earthquake



Ice Velocities

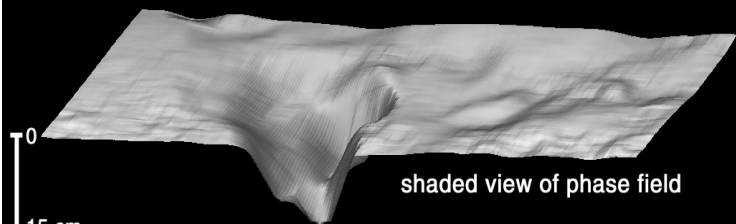


Ground subsidence near Pomona, California

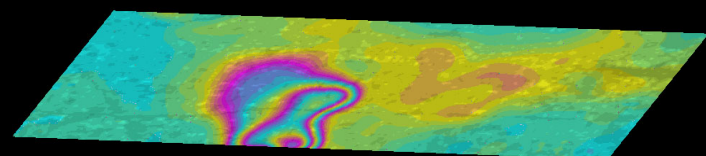
Time interval: 20 Oct 93 - 22 Dec 95



distorted AAA street map



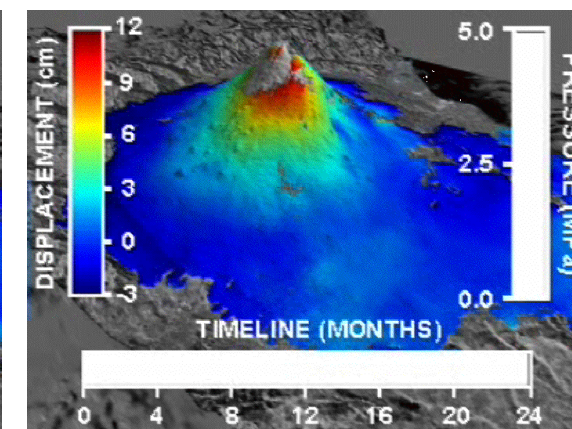
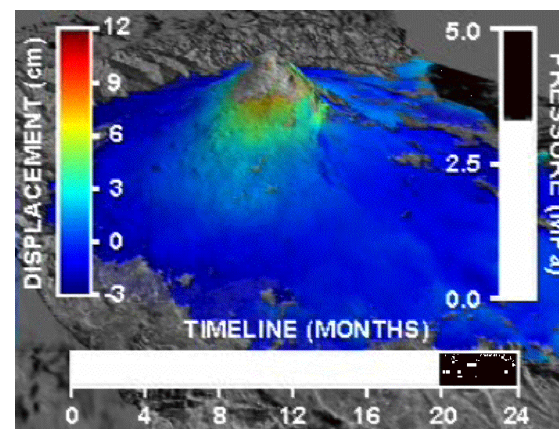
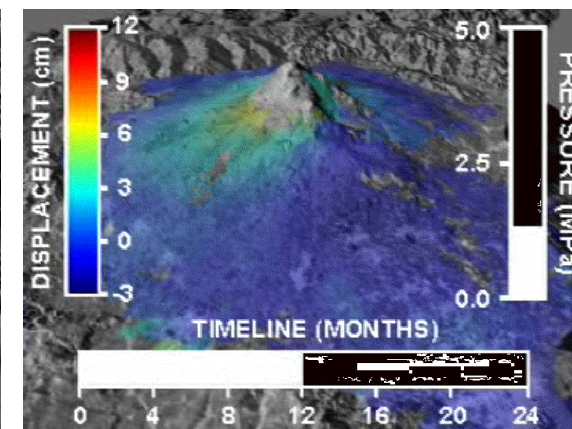
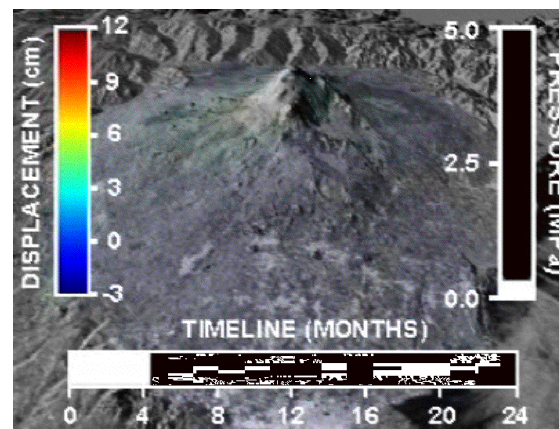
shaded view of phase field



ERS-1, 3-pass interferogram

G. Peltzer, 1997 - JPL

Etna Volcano



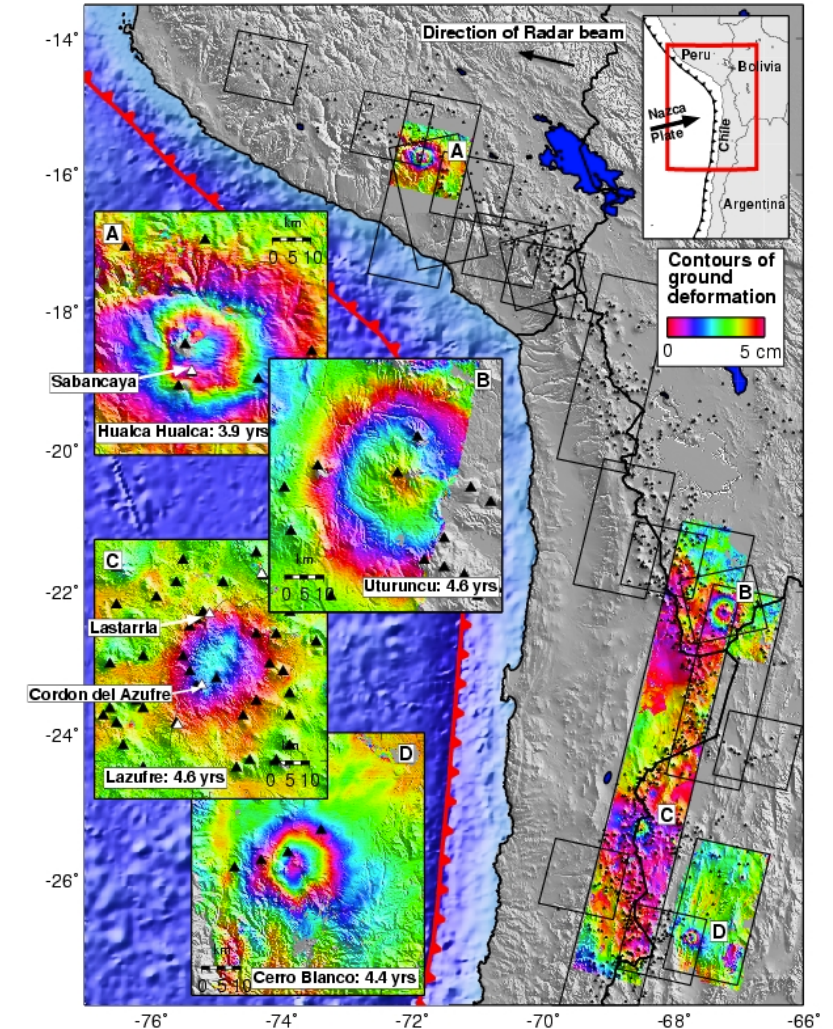
Joughin et al, 1999

Slide modified from Paul Rosen (JPL)



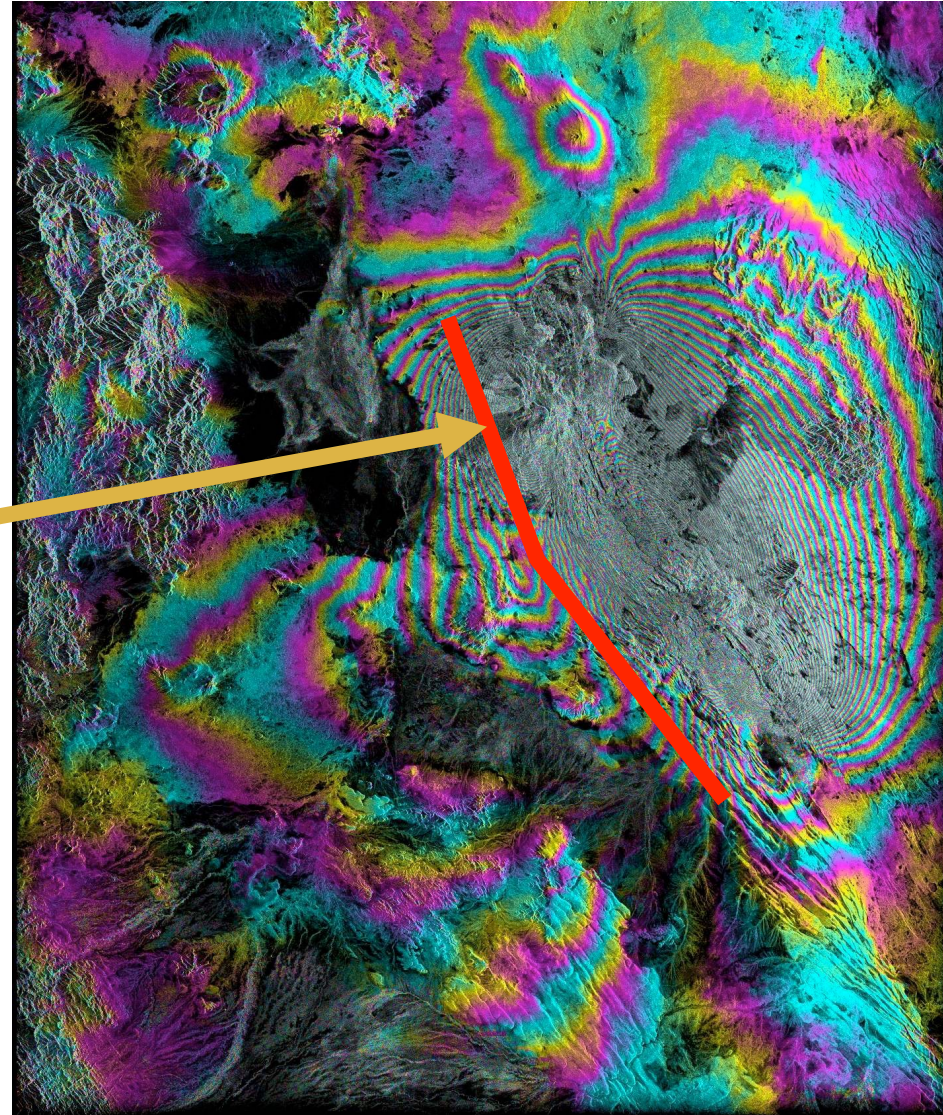
Volcanoes of the Central Andes

- Map of deformation in and around volcanoes
- European ERS-1 and ERS-2 satellites (C-band)
- Some related to recent eruptions
- Others were not known to be active now
- M. Pritchard (now at Cornell)



Asal Rift Dike Injection

6 May – 28 Oct 2005

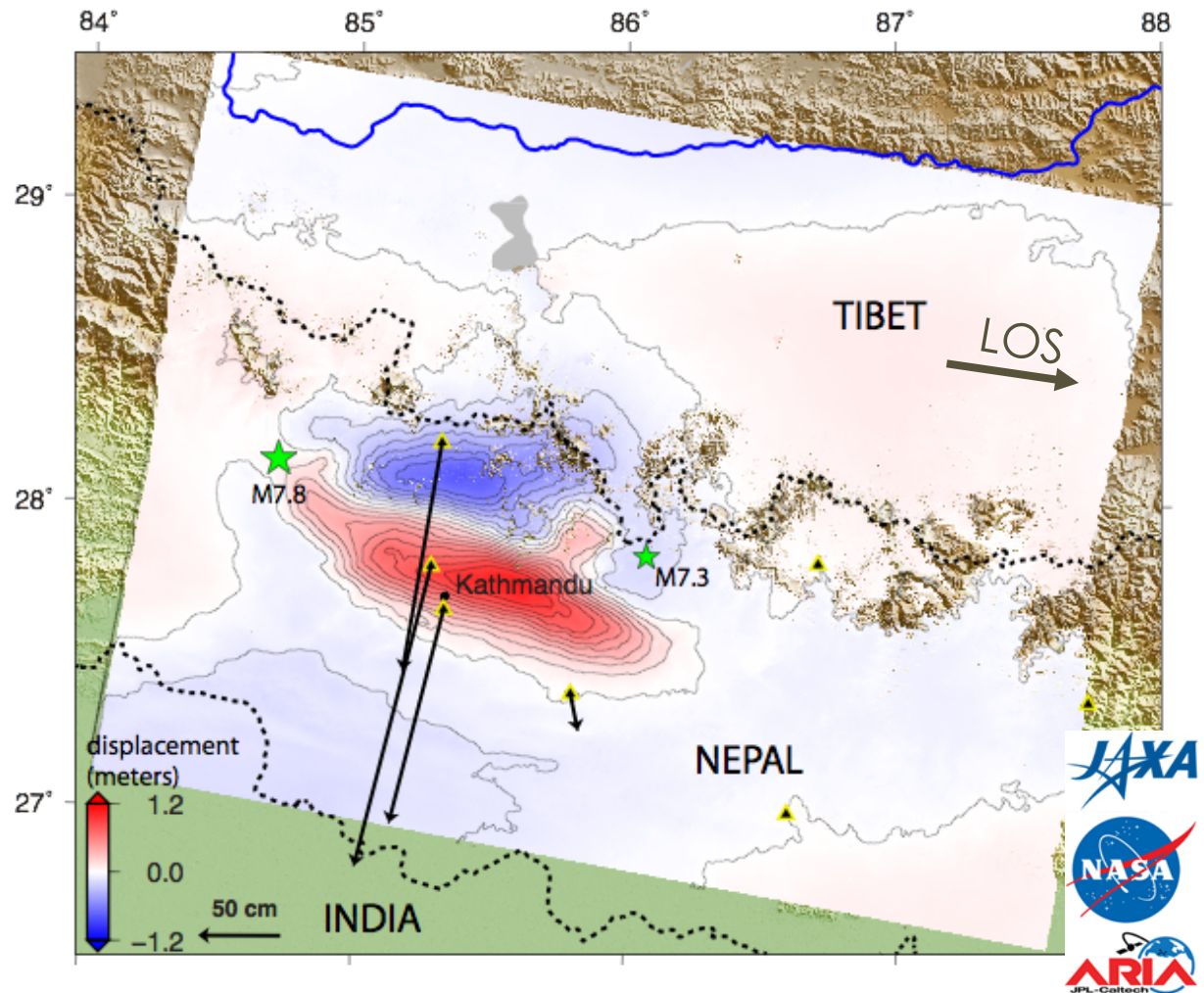


Tim Wright, U. Leads



2015 M7.8 Gorkha Earthquake in Nepal

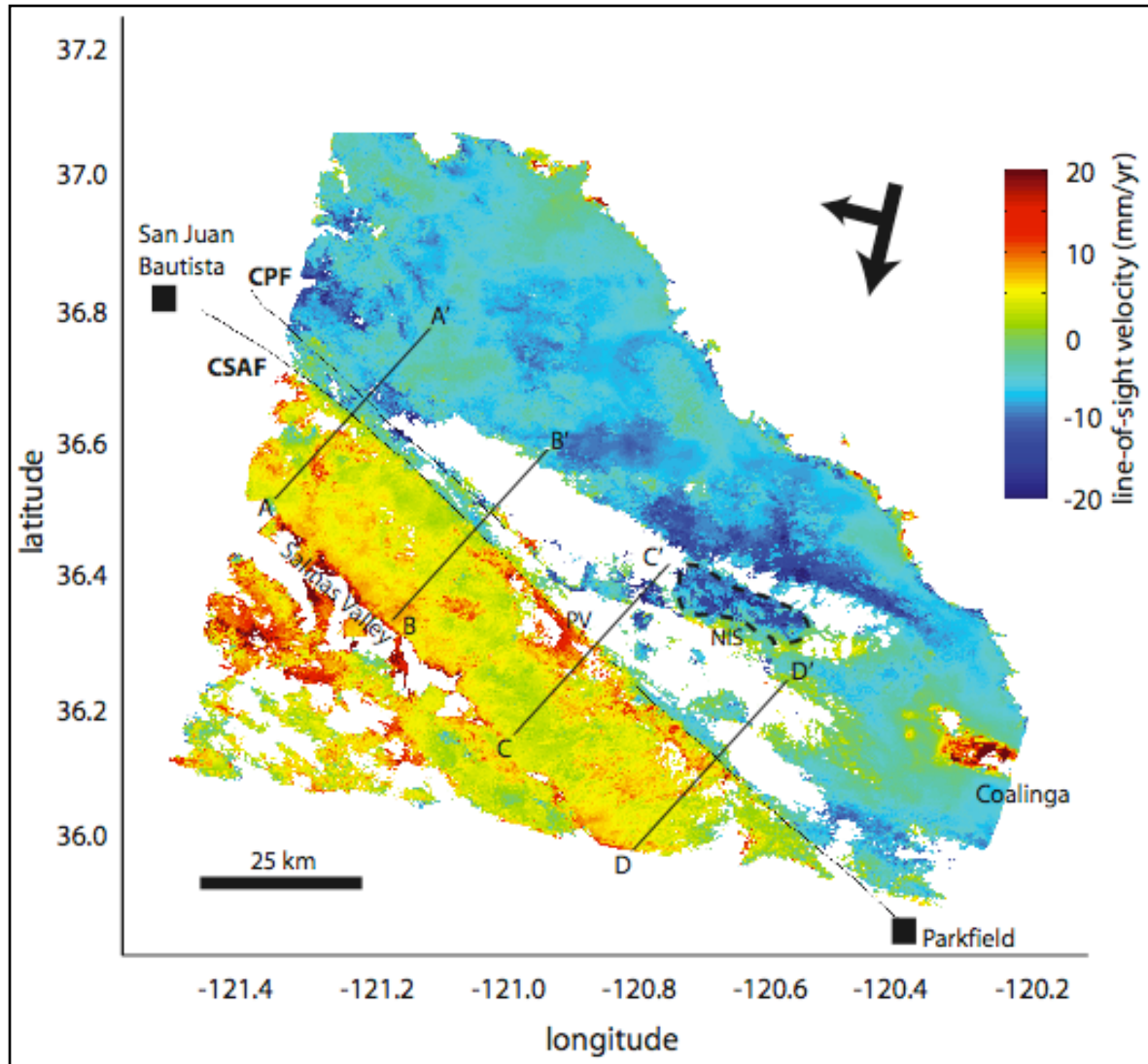
- ALOS-2 ScanSAR interferogram
- Descending line-of-sight (LOS) perpendicular to horizontal
- InSAR phase only sees vertical component
- High Himalayas dropped down as much as 1.2 m
- Yue, H., et al. (2016, in press), Depth varying rupture properties during the 2015 Mw 7.8 Gorkha (Nepal) earthquake, Tectonophysics, doi:10.1016/j.tecto.2016.07.005.



GPS data from Galetzka, J., et al. (2015), Slip pulse and resonance of the Kathmandu basin during the 2015 Gorkha earthquake, Nepal, *Science*, 349 (6252), 1091-1095



Creep on the San Andreas Fault



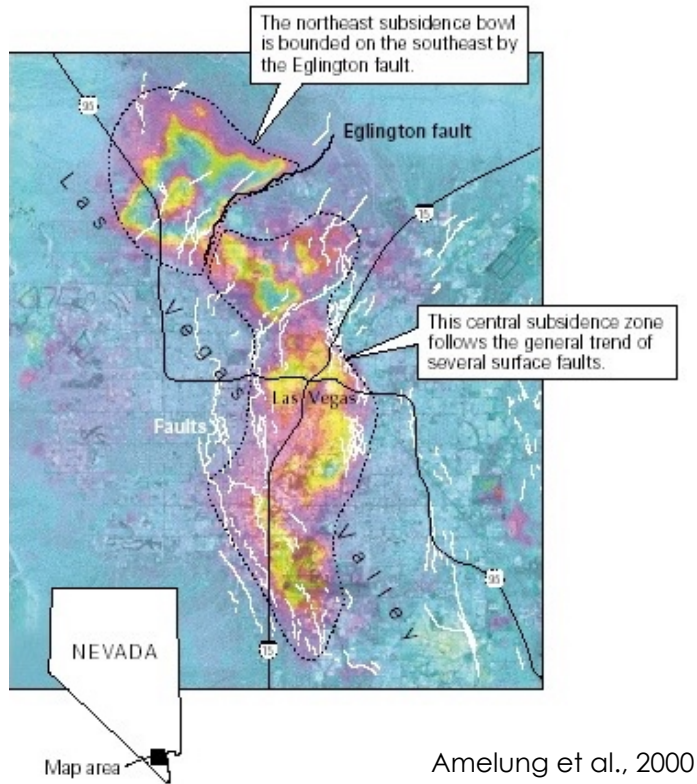
Stack of 12 ERS interferograms
spanning May 1992-Jan 2001

Figures from Isabelle Ryder, U.C. Berkeley

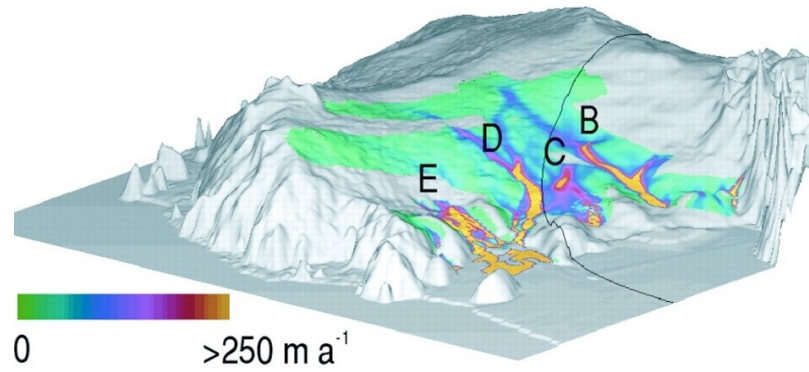


Some of InSAR's Greatest Hits

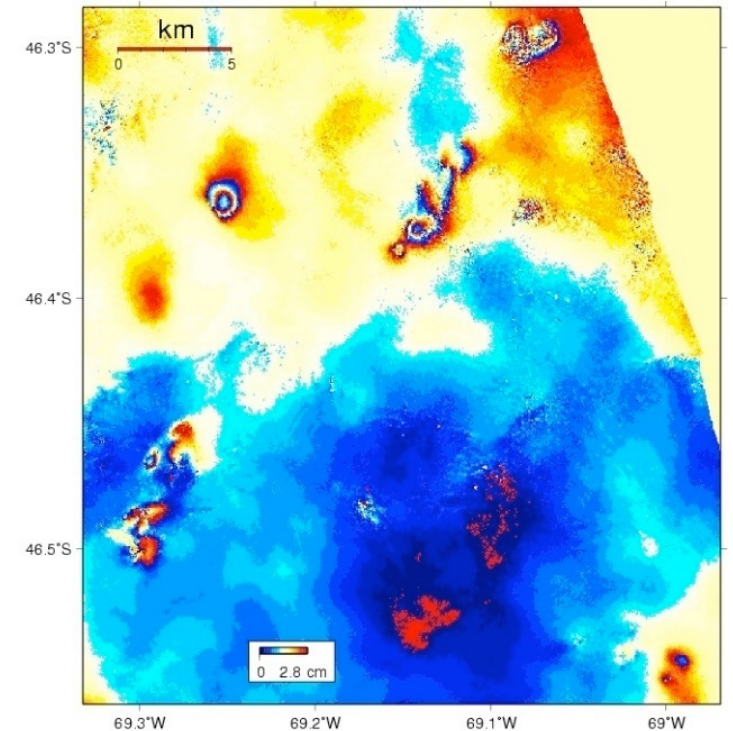
The Ups and Downs of Las Vegas (from groundwater pumping)



Antarctica Ice Stream Velocities from InSAR/Feature Tracking



Enhanced Oil Recovery Detected in the San Jose Basin, Argentina

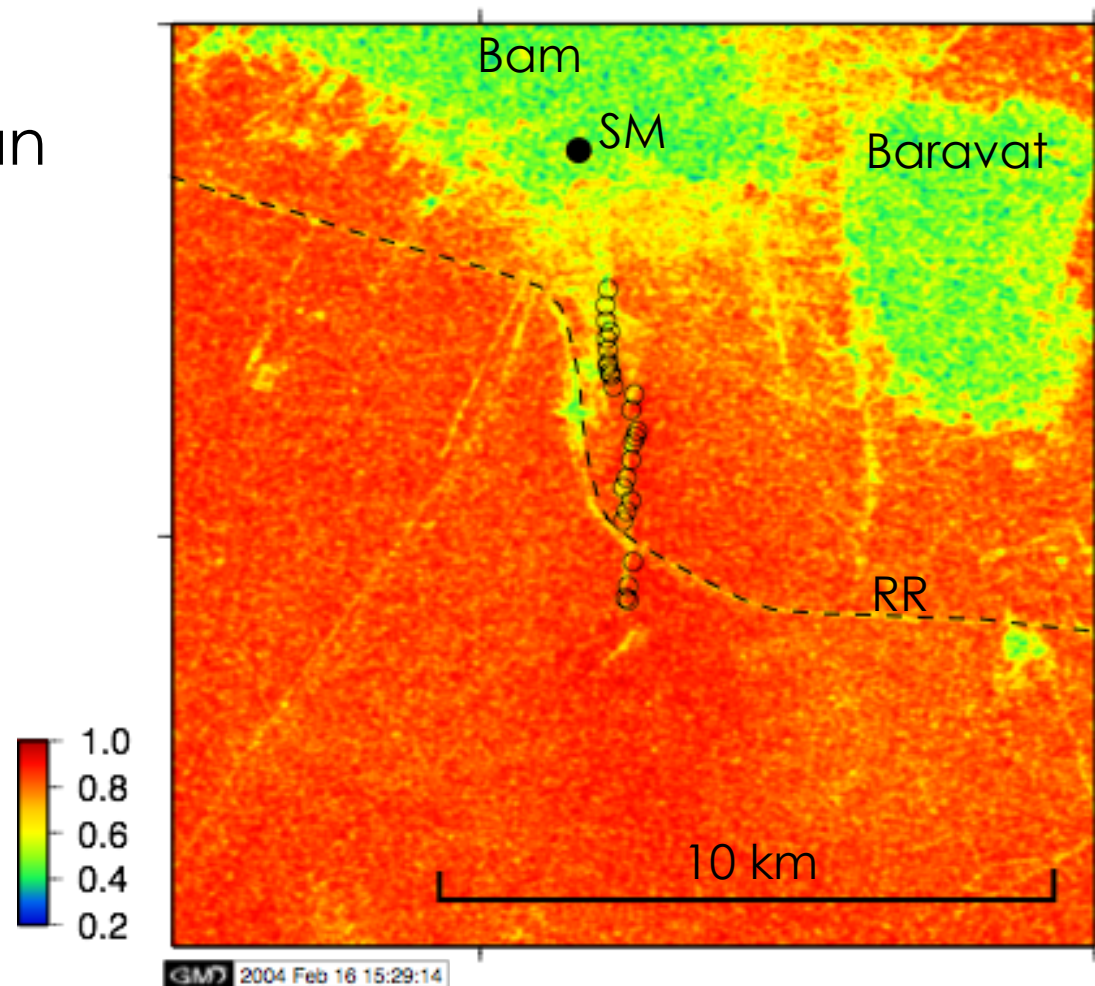


Slide Modified from Matt Pritchard (Cornell)



Decorrelation Shows Surface Ruptures

2003 M6.5 Bam
earthquake in Iran

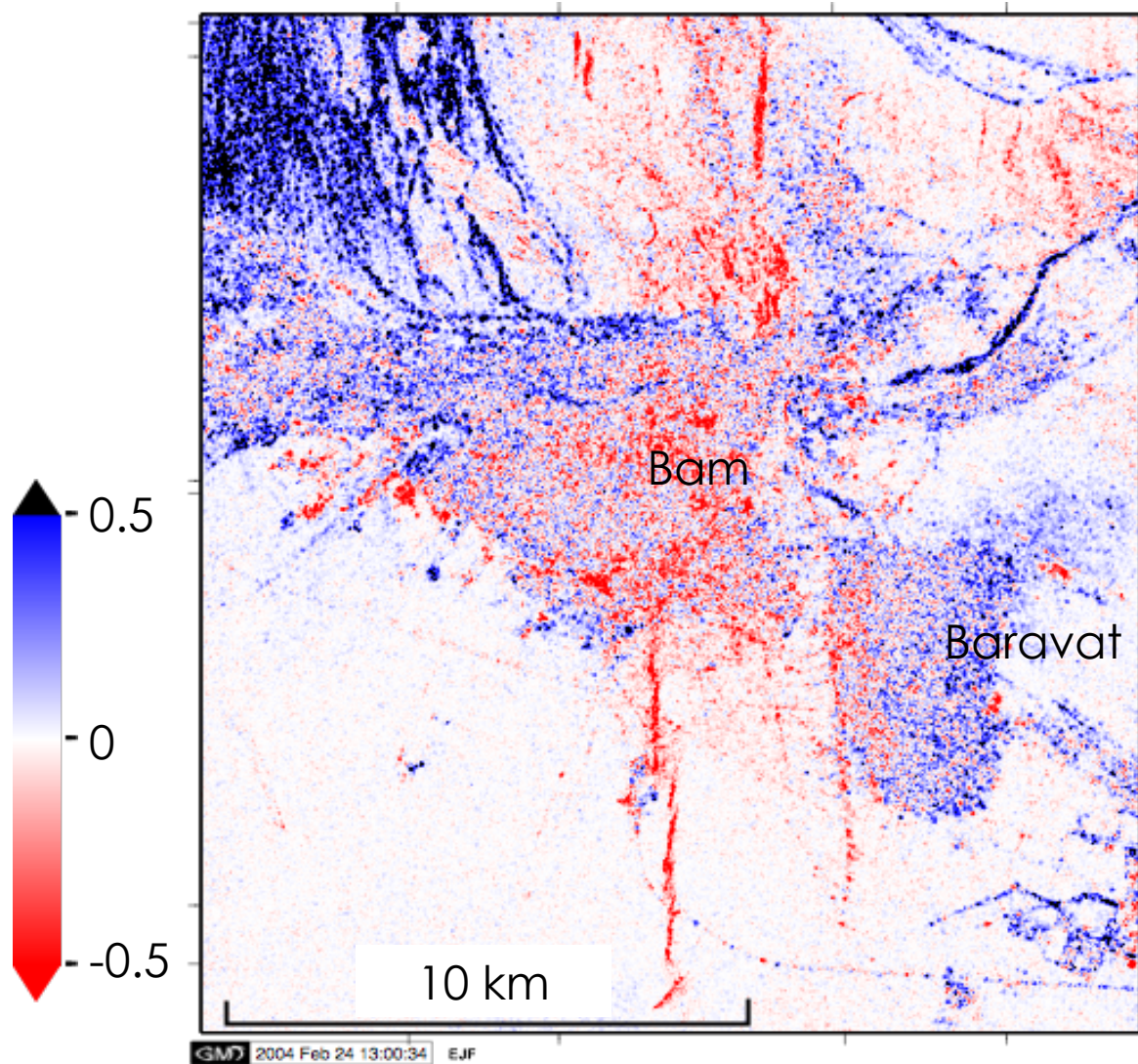


- 35 days
- 3 Dec 2003 – 7 Jan 2014
- Envisat
- Descending track
- 8perp 580 m

Fielding, E. J., M. Talebian, P. A. Rosen, H. Nazari, J. A. Jackson, M. Ghorashi, and R. Walker (2005), Surface ruptures and building damage of the 2003 Bam, Iran, earthquake mapped by satellite synthetic aperture radar interferometric correlation, *J. Geophys. Res.*, 110(B3), B03302, doi:10.1029/2004JB003299.



Correlation Change

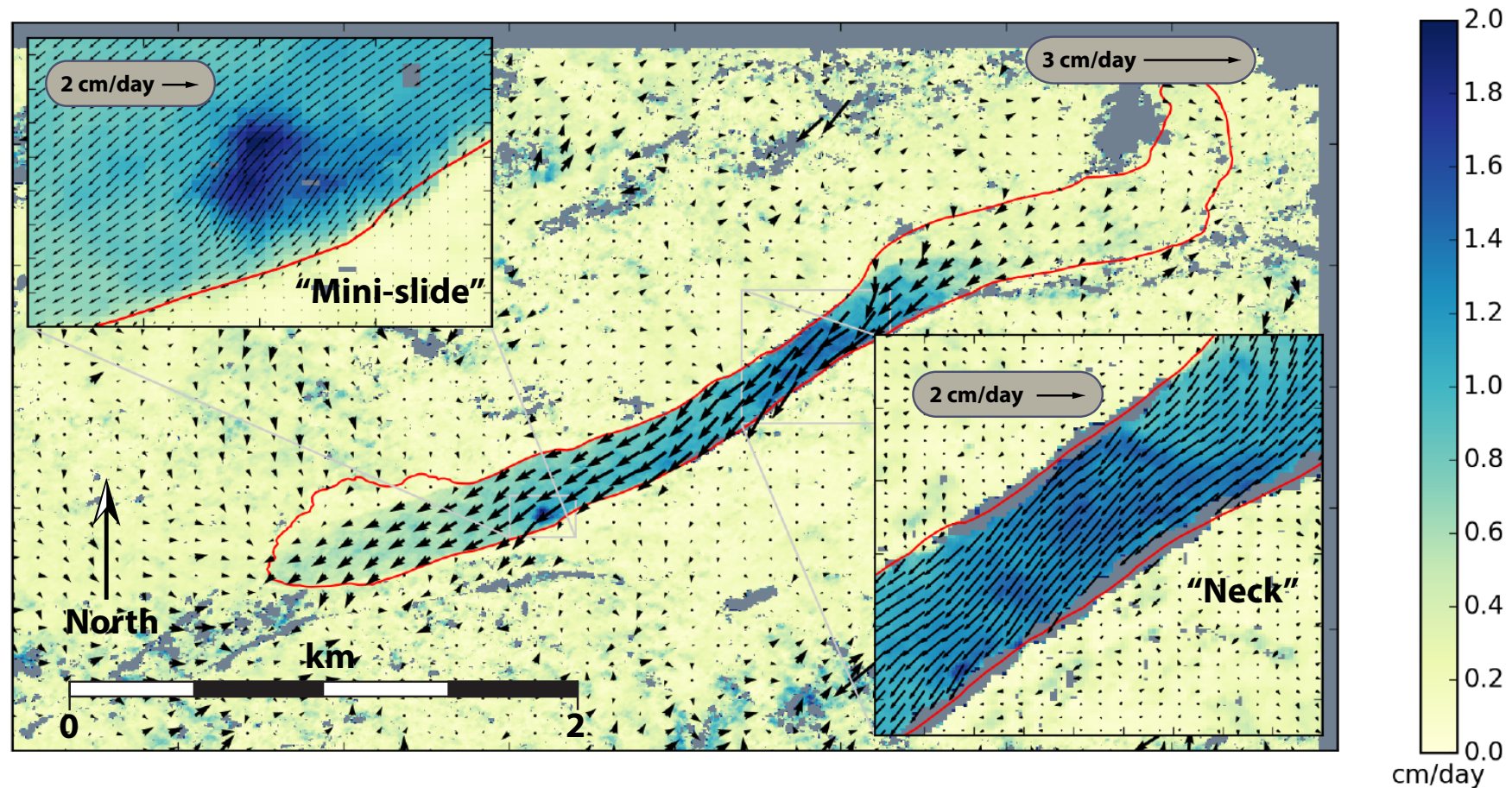


- co-seismic correlation minus pre-seismic correlation
- red is co-seismic decorrelation



Landslide Motion

Combination of four NASA UAVSAR InSAR flight lines



Delbridge, B. G., R. Bürgmann, E. Fielding, S. Hensley, and W. H. Schulz (2016), Three-dimensional surface deformation derived from airborne interferometric UAVSAR: Application to the Slumgullion Landslide, *J. Geophys. Res. Solid Earth*, 121(5), 3951–3977, doi:10.1002/2015JB012559.



NASA-ISRO SAR Mission (NISAR)

- High spatial resolution with frequent revisit time
- Earliest baseline launch date: 2021
- Dual frequency L- and S-band SAR
- L-band SAR from NASA and S-band SAR from ISRO
- 3 years science operations (5+ years consumables)
- All science data will be made available free and open
- <https://nisar.jpl.nasa.gov>

Slide courtesy of Paul Rosen (JPL)

NISAR Characteristic:	Would Enable:
L-band (24 cm wavelength)	Low temporal decorrelation and foliage penetration
S-band (12 cm wavelength)	Sensitivity to light vegetation
SweepSAR technique with Imaging Swath >240 km	Global data collection
Polarimetry (Single/Dual/Quad)	Surface characterization and biomass estimation
12-day exact repeat	Rapid Sampling
3-10 meters mode-dependent SAR resolution	Small-scale observations
3 years since operations (5 years consumables)	Time-series analysis
Pointing control < 273 arcseconds	Deformation interferometry
Orbit control < 500 meters	Deformation interferometry
>30% observation duty cycle	Complete land/ice coverage
Left/Right pointing capability	Polar coverage, North and South
Noise Equivalent Sigma Zero \leq -23 db	Surface characterization of smooth surfaces

